24th INTERNATIONAL CONGRESS ON SOUND AND VIBRATION
23–27 July 2017, London

ICSV24
23-27JULY 2017
LONDON CALLING

LOCAL ACTIVE SOUND CONTROL USING THE REMOTE MICROPHONE TECHNIQUE AND HEAD-TRACKING FOR TONAL AND BROADBAND NOISE SOURCES

Woomin Jung, Stephen J. Elliott and Jordan Cheer
Institute of Sound and Vibration Research, University of Southampton, UK
email: wj3e13@soton.ac.uk

Local active sound control can be combined with the remote microphone technique and head-tracking for the case when direct measurement of the error signals at a listener's ears is not possible and the position of the listener's head is continuously changing. This paper presents the performance of the combined active control system when it is applied to reduce either tonal or broadband random noise. First of all, effects of the combined system were experimentally investigated when periodic noise from a single primary source was adaptively controlled in real time. By directly applying observation filters and acoustical responses in the frequency domain, it was shown that active control of tonal noise can be effectively improved by the remote microphone technique and head-tracking. In addition, the ability of the combined active control system to control stationary random broadband noise was investigated. However, in this case, the causality of the observation filter must be considered due to the unpredictability of random noise. Therefore, the causally constrained remote microphone technique and the corresponding broadband active noise control system were studied.

Keywords: remote microphone technique, head-tracking

1. Introduction

The active headrest system, in which secondary loudspeakers and error microphones are installed around a headrest of a vehicle seat, has been suggested as a practical local active control system to reduce the interior noise around the ears of the driver and passengers [1] [2]. However, when direct measurement of the error signals at a listener's ears is not possible, this can be a constraint on the application of the active headrest system. Especially, because a small zone of quiet is generated at higher frequencies, the separation between the ears and the error microphones can degrade the attenuation performance around the ears. To overcome this limitation, a shift of the zone of quiet has been suggested by a number of virtual sensing algorithms [3] [4] [5]. Among these algorithms, the remote microphone technique has been investigated for the nearfield estimation of signals at the virtual error microphones from measured signals at remotely installed monitoring microphones through simulations and off-line analysis from measured data [6]. The present paper investigates the accuracy of the remote microphone techniques through both real-time experiments for tonal sounds and off-line analysis for stationary random broadband sounds.

As another practical issue, head movements of the listener can produce changes in sound fields and acoustic responses. To prevent these changes from degrading the convergence stability and attenuation performance of the adaptive active headrest system, the application of head-tracking has been suggested [6]. In previous research, off-line test results in the frequency domain have shown

that the head-tracking can improve the stability and attenuation performance of the active headrest system when the listener's head is moving [6]. In this paper, a complete active headrest system combined with both the remote microphone technique and a commercial head-tracking device is used to adaptively control tonal sounds.

In Section 2, a theoretical analysis for the integrated active headrest system is presented in the frequency domain for controlling tonal disturbances and an analysis in time domin is also included for a causal controller designed for broadband random disturbances. In Section 3, real-time experiments demonstrate the ability of the nearfield estimation and integrated active headrest system to reduce tonal noise. Section 3 also describes results of off-line analysis with measured acoustic responses when the causal filters for the remote microphone technique and active control are applied to reduce broadband random sounds. Finally, in Section 4, conclusions are drawn.

2. The nearfield estimation and integrated active control system

2.1 Frequency domain analysis

When the remote microphone technique is combined with a feedforward active control system, the block diagram of the combined algorithm is shown in Fig. 1. This combined active control system is initially investigated in the frequency domain in this section. Results in the frequency domain allow a straightforward assessment of both the nearfield estimation and attenuation performance when it aims to reduce tonal noise regardless of the causality constraint.

In Fig. 1, the primary sources, which have a vector of source strengths $\mathbf{v}^T = [v_1, v_2 \ \dots \ v_{N_v}]$, produce a vector of disturbance signals $\mathbf{d}_e^T = [d_{e1}, d_{e2} \ \dots \ d_{eN_e}]$ at the virtual error microphones and a vector of reference signals $\mathbf{x}^T = [x_1, x_2 \ \dots \ x_{N_x}]$ at the reference microphones via the matrices of transfer responses $\mathbf{P}_e$ and $\mathbf{R}$, respectively. As the reference sensor signals drive the matrix of the active control filter, $\mathbf{W}$, to produce a vector of control signals $\mathbf{u}^T = [u_1, u_2 \ \dots \ u_{N_u}]$, the control signals are transmitted to the virtual error microphones, via the matrix of plant responses $\mathbf{G}_e$. A vector of error signals, $\mathbf{e}$, at the virtual error microphones after control can be thus defined as

$$\mathbf{e} = \mathbf{d}_e + \mathbf{G}_e\mathbf{u} = \mathbf{d}_e + \mathbf{G}_e\mathbf{W}\mathbf{x} = \mathbf{P}_e\mathbf{v} + \mathbf{G}_e\mathbf{W}\mathbf{R}\mathbf{v}. \tag{1}$$

When it is necessary to estimate the virtual error signals, $\mathbf{e}$, from the monitoring microphone signals $\mathbf{m}^T = [m_1, m_2 \ \dots \ m_{N_m}]$, which are defined as

$$\mathbf{m} = \mathbf{d}_m + \mathbf{G}_m\mathbf{u} = \mathbf{d}_m + \mathbf{G}_m\mathbf{W}\mathbf{x} = \mathbf{P}_m\mathbf{v} + \mathbf{G}_m\mathbf{W}\mathbf{R}\mathbf{v}, \tag{2}$$

where $\mathbf{d}_m^T = [d_{m1}, d_{m2} \ \dots \ d_{mN_m}]$ is a vector of disturbance signals at the monitoring microphones and $\mathbf{G}_m$ is the matrix of plant responses between the secondary sources and the monitoring microphones, the estimated error signals, $\hat{\mathbf{e}}$, at the virtual error microphones can be written as

$$\hat{\mathbf{e}} = \hat{\mathbf{d}}_e + \hat{\mathbf{G}}_e\mathbf{u} = \hat{\mathbf{O}}\hat{\mathbf{d}}_m + \hat{\mathbf{G}}_e\mathbf{u} = \hat{\mathbf{O}}(\mathbf{m} - \hat{\mathbf{G}}_m\mathbf{u}) + \hat{\mathbf{G}}_e\mathbf{u}, \tag{3}$$

where the superscript ^ represents an estimate of an actual value and $\hat{\mathbf{O}}$ is the linear observation filter used to estimate $\hat{\mathbf{d}}_e$ from $\hat{\mathbf{d}}_m$.

Since the active control system attempts to minimise the estimated error signals, $\hat{\mathbf{e}}$, the accuracy of the nearfield estimation with the observation filter, $\hat{\mathbf{O}}$, can be a important factor for better attenuation at the error microphones. Previous research has shown that when the number of monitoring microphones (N_m) is larger than the number of error microphones (N_e), the problem is mathematically overdetermined, the optimal observation filter, $\mathbf{O}_{\text{opt}}$, is given as

$$\mathbf{O}_{\text{opt}} = \mathbf{S}_{d_m d_e}(\mathbf{S}_{d_m d_m} + \beta\mathbf{I})^{-1} = \mathbf{P}_e\mathbf{S}_{vv}\mathbf{P}_m^H(\mathbf{P}_m\mathbf{S}_{vv}\mathbf{P}_m^H + \beta\mathbf{I})^{-1}, \tag{4}$$

where $\mathbf{S}_{d_m d_e} = E[\mathbf{d}_e \mathbf{d}_m^H]$ is the cross spectral density matrix between $\mathbf{d}_m$ and $\mathbf{d}_e$, $\mathbf{S}_{d_m d_m} = E[\mathbf{d}_m \mathbf{d}_m^H]$ is the power spectral density matrix for $\mathbf{d}_m$ when $E[\,]$ is the expectation operator and ^{H} is the Hermitian, complex conjugate transpose, and β is a positive real effort-weighting parameter to improve the robustness of the optimal observation filter and $\mathbf{I}$ is the identity matrix having the same dimensions as $\mathbf{S}_{d_m d_m}$ [4] [6]. If $\mathbf{S}_{vv}$ is the power spectral density matrix of primary source strengths, $\mathbf{O}_{\text{opt}}$, can be written in the alternative form on the right-hand side of Eq. (4). From Eq. (4), the optimal observation filter, $\mathbf{O}_{\text{opt}}$, can be calculated from pre-measured data of $\mathbf{d}_e$ and $\mathbf{d}_m$ before active control.

To calculate the optimal active controller, $\mathbf{W}_{\text{opt}}$, by substituting Eq. (2) into Eq. (3), Eq. (3) can be expressed as

$$\hat{\mathbf{e}} = \hat{\mathbf{O}}\mathbf{d}_m + \left[\hat{\mathbf{G}}_e + \hat{\mathbf{O}}(\mathbf{G}_m - \hat{\mathbf{G}}_m)\right]\mathbf{W}\mathbf{x}. \tag{5}$$

In Eq. (5), the term, $\hat{\mathbf{G}}_e + \hat{\mathbf{O}}(\mathbf{G}_m - \hat{\mathbf{G}}_m)$ can be defined as the effective plant response, $\mathbf{G}$, between $\mathbf{u}$ and $\hat{\mathbf{e}}$. By minimising the cost function, which is defined as $J_1 = trace\left\{E\left[\hat{\mathbf{e}}\,\hat{\mathbf{e}}^H\right]\right\}$, the optimal active controller, $\mathbf{W}_{\text{opt}}$ can be obtained using the derivation detailed in Ref. [1] [4] as

$$\mathbf{W}_{\text{opt}} = -(\mathbf{G}^H\mathbf{G})^{-1}\mathbf{G}^H\mathbf{O}_{\text{opt}}\mathbf{S}_{xd_m}\mathbf{S}_{xx}^{-1}, \tag{6}$$

where the optimal observation filter, $\mathbf{O}_{\text{opt}}$, is applied and $\mathbf{S}_{xd_m} = E[\mathbf{d}_m\mathbf{x}^H]$ is the cross spectral density matrix between $\mathbf{d}_m$ and $\mathbf{x}$, $\mathbf{S}_{xx} = E[\mathbf{x}\mathbf{x}^H]$ is the power spectral density matrix for $\mathbf{x}$.

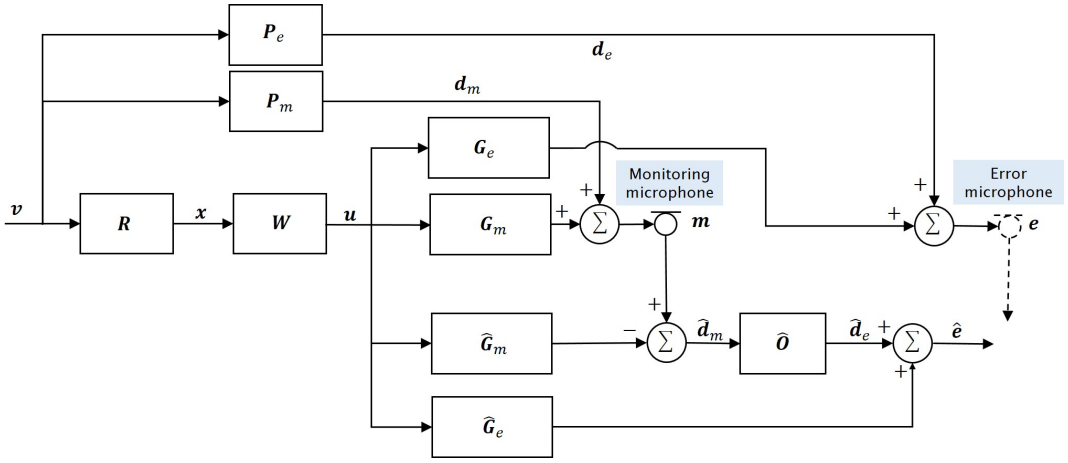

Figure 1: Block diagram of the feedforward active control algorithm, combined with the remote microphone technique.

2.2 Time domain analysis

For stationary random broadband noise, it is required that the observation filter and the active controller are causally constrained due to the unpredictability of random noise. Therefore, we will investigate the nearfield estimation and attenuation performance in the time domain.

In Fig. 1, a vector of N_x reference sensor signals in the time domain, at the nth sample time is expressed as $\boldsymbol{x}(n)^T = [x_1(n), x_2(n)\ \ldots\ x_{N_x}(n)]$ and a vector of control signals for the N_u secondary sources is described as $\boldsymbol{u}(n)^T = [u_1(n), u_2(n)\ \ldots\ u_{N_u}(n)]$ from the controller which is the Ith order FIR filter with coefficients, $w_{n_u n_x i}$. In addition, the matrix of plant responses, $\mathbf{G}_e$ is described by the Jth order FIR filters with arbitrary accuracy, which have the impluse response from the n_uth secondary source to the n_eth error microphone as $g_{e,n_e n_u j}$. The vectors of error signals and disturbance signals for N_e error microphones are $\boldsymbol{e}(n)^T = [e_1(n), e_2(n)\ \ldots\ e_{N_e}(n)]$ and

$\boldsymbol{d}_e(n)^T = [d_{e1}(n), d_{e2}(n)\ \ldots\ d_{eN_e}(n)]$, respectively and thus the n_eth error microphone signal can be written as [1]

$$e_{n_e}(n) = d_{en_e} + \sum_{n_u=1}^{N_u}\sum_{j=0}^{J-1}\sum_{n_x=1}^{N_x}\sum_{i=0}^{I-1} g_{e,n_e n_u j} w_{n_u n_x i} x_{n_x}(n-i-j). \tag{7}$$

When the $N_e N_u N_x$ filtered-reference signals for the error microphones are written as

$$r_{e,n_e n_u n_x}(n) = \sum_{j=0}^{J-1} g_{e,n_e n_u j} x_{n_x}(n-j), \tag{8}$$

Eq. (7) can be expressed by substituting Eq. (8) into Eq. (7) as

$$e_{n_e}(n) = d_{en_e} + \sum_{i=0}^{I-1} \boldsymbol{w}_i^T \boldsymbol{r}_{en_e}(n-i), \tag{9}$$

where $\boldsymbol{w}_i^T = [w_{11i}\ w_{12i}\ \ldots\ w_{1N_x i}\ w_{21i}\ w_{22i}\ \ldots\ w_{N_u N_x i}]$ and $\boldsymbol{r}_{en_e}^T = [r_{e,n_e 11}\ r_{e,n_e 12}\ \ldots\ r_{e,n_e 1N_x}\ r_{e,n_e 21}\ r_{e,n_e 22}\ \ldots\ r_{e,n_e N_u N_x}]$. Therefore, the vector of signals at the error microphones in time domain can be expressed as

$$\boldsymbol{e}(n) = \boldsymbol{d}_e(n) + \boldsymbol{R}_e(n)\boldsymbol{w}(n), \tag{10}$$

where

$$\boldsymbol{R}_e(n) = \begin{pmatrix} \boldsymbol{r}_{e1}^T(n) & \boldsymbol{r}_{e1}^T(n-1) & \cdots & \boldsymbol{r}_{e1}^T(n-I+1) \\ \boldsymbol{r}_{e2}^T(n) & \boldsymbol{r}_{e2}^T(n-1) & \cdots & \boldsymbol{r}_{e2}^T(n-I+1) \\ \vdots & \vdots & \ddots & \vdots \\ \boldsymbol{r}_{en_e}^T(n) & \boldsymbol{r}_{en_e}^T(n-1) & \cdots & \boldsymbol{r}_{en_e}^T(n-I+1) \end{pmatrix}, \tag{11}$$

and $\boldsymbol{w}(n) = [\boldsymbol{w}_0^T\ \boldsymbol{w}_1^T\ \ldots\ \boldsymbol{w}_{I-1}^T]^T$. Similarly, the vector of signals at the N_m monitoring microphones, $\boldsymbol{m}(n)^T = [m_1(n), m_2(n)\ \ldots\ m_{N_m}(n)]$ is defined as

$$\boldsymbol{m}(n) = \boldsymbol{d}_m(n) + \boldsymbol{R}_m(n)\boldsymbol{w}(n), \tag{12}$$

where $\boldsymbol{d}_m(n)^T = [d_{m1}(n), d_{m2}(n)\ \ldots\ d_{mN_m}(n)]$ and $\boldsymbol{R}_m(n)$ have a similar form to $\boldsymbol{R}_e(n)$ in Eq. (11), except that the impluse response from the n_uth secondary source to the n_mth monitoring microphone, $g_{m,n_m n_u j}$ is used in Eq. (8), instead of $g_{e,n_e n_u j}$.

The vector of estimated error signals in the time domain, $\hat{\boldsymbol{e}}(n)$, following a similar process to Eq. (3), can be written as

$$\hat{\boldsymbol{e}}(n) = \hat{\boldsymbol{d}}_e(n) + \hat{\boldsymbol{R}}_e(n)\boldsymbol{w}(n) = \hat{\boldsymbol{O}}(n)\{\boldsymbol{m}(n) - \hat{\boldsymbol{R}}_m(n)\boldsymbol{w}(n)\}' + \hat{\boldsymbol{R}}_e(n)\boldsymbol{w}(n), \tag{13}$$

where $\hat{\boldsymbol{O}}(n)$ is the matrix of observation filter coefficients in the time domain, which is defined as $\hat{\boldsymbol{O}}(n) = [\boldsymbol{O}_1^T\ \boldsymbol{O}_2^T\ \ldots\ \boldsymbol{O}_{N_e}^T]^T$ and $\boldsymbol{O}_{n_e} = [\boldsymbol{O}_{n_e 1}^T\ \boldsymbol{O}_{n_e 2}^T\ \ldots\ \boldsymbol{O}_{n_e N_m}^T]^T$ and $\{\ \}'$ represents the $JN_m \times 1$ vector of values between the braces when the impulse response from the n_mth monitoring microphone to the n_eth error microphone, $\boldsymbol{O}_{n_e n_m}$ is modelled by an FIR filter with J filter coefficients as

$$\boldsymbol{O}_{n_e n_m} = [O_{n_e n_m 0}\ O_{n_e n_m 1}\ \ldots\ O_{n_e n_m (J-1)}]^T. \tag{14}$$

The matrix of the optimal observation filter conefficients in the time domain, $\boldsymbol{O}_{opt}$ can be obtained using the derivation detailed in Ref.[4] as

$$\boldsymbol{O}_{opt} = \left(\{E[\boldsymbol{d}_m'(n)\boldsymbol{d}_m'^T(n)] + \beta\mathbf{I}'\}^{-1}\{E[\boldsymbol{d}_m'(n)\boldsymbol{d}_e^T(n)]\}\right)^T, \tag{15}$$

where $\boldsymbol{d}_m^{'}(n)$ also represents the $JN_m \times 1$ vector, which is defined as $\boldsymbol{d}_m^{'}(n) = [\boldsymbol{d}_{m1}^{'T}(n)\ \boldsymbol{d}_{m2}^{'T}(n)\ \ldots\ \boldsymbol{d}_{mN_m}^{'T}(n)]^T$ and $\boldsymbol{d}_{mn_m}^{'}(n) = [d_{mn_m}(n)\ d_{mn_m}(n-1)\ \ldots\ d_{mn_m}(n-J-1)]^T$, and $\mathbf{I}^{'}$ is the identity matrix having the same dimensions as $E[\boldsymbol{d}_m^{'}(n)\boldsymbol{d}_m^{'T}(n)]$.

To calculate the causally constrained optimal controller, $\boldsymbol{w}_{opt}$, in time domain to minimise the cost function, $J_2 = trace\left\{ E\left[\hat{\boldsymbol{e}}(n)\ \hat{\boldsymbol{e}}^T(n)\right] \right\}$, it is required that Eq. (13) is expressed in terms of $\boldsymbol{w}(n)$ by substituting Eq. (12) into Eq. (13) as

$$\hat{\boldsymbol{e}}(n) = \hat{\boldsymbol{O}}(n)\boldsymbol{d}_m^{'}(n) + [\hat{\boldsymbol{O}}(n)\Delta\boldsymbol{R}_m^{'}(n) + \hat{\boldsymbol{R}}_e(n)]\boldsymbol{w}(n), \tag{16}$$

where $\Delta\boldsymbol{R}_m^{'}(n)\boldsymbol{w}(n) = \{[\boldsymbol{R}_m(n) - \hat{\boldsymbol{R}}_m(n)]\boldsymbol{w}(n)\}^{'}$. Therefore, the causally constrained optimal controller, $\boldsymbol{w}_{opt}$, with the optimal observation filter, $\boldsymbol{O}_{opt}$, can be given by [1] [4]

$$\boldsymbol{w}_{\text{opt}} = -\{E[\boldsymbol{R}^T(n)\boldsymbol{R}(n)]\}^{-1}E[\boldsymbol{R}^T(n)\boldsymbol{O}_{\text{opt}}\boldsymbol{d}_m^{'}(n)], \tag{17}$$

where $\boldsymbol{R} = [\boldsymbol{O}_{opt}\Delta\boldsymbol{R}_m^{'}(n) + \hat{\boldsymbol{R}}_e(n)]$.

2.3 Head-tracking for local active sound control

When the position of a listener's head is continuously changing, the head-tracking technology can allow the local active control system combined with the remote microphone technique to improve the attenuation performance and convergence stability, as suggested by previous research [6].

If $\hat{\mathbf{G}}_e$, $\hat{\mathbf{G}}_m$ and $\mathbf{O}_{\text{opt}}$ in Eq. (6) and $\hat{\boldsymbol{R}}_e(n)$, $\hat{\boldsymbol{R}}_m(n)$ and $\boldsymbol{O}_{opt}$ in Eq. (17) are only defined at a single fixed position, then head movements produce differences between the actual and estimated error signals and thus degrade the attenuation performance at the error microphones. To overcome this problem, the active headrest system can be designed to use the head position information, which is given by a head-tracking device, to update $\hat{\mathbf{G}}_e$, $\hat{\mathbf{G}}_m$ and $\mathbf{O}_{\text{opt}}$ for tonal control and $\hat{\boldsymbol{R}}_e(n)$, $\hat{\boldsymbol{R}}_m(n)$ and $\boldsymbol{O}_{opt}$ for broadband random control from a pre-calculated lookup table for different head positions.

3. Experimental investigation

3.1 Experimental arrangement

Fig. 2 shows the experimental installation used for measuring acoustic responses and the real-time implementation in an anechoic chamber. Four monitoring microphones were installed, with two on the back of the headrest and two on the supporting structure, as shown in Fig. 2. The positions of these monitoring microphones were carefully selected through a series of preliminary experiments to obtain an accurate nearfield estimation of the disturbance signals at the virtual error sensors. To compare the estimated disturbance signals at the virtual error microphones with the actual disturbance signals, two microphones were also installed in the ears of a dummy head. The dummy head and physical error microphones can be removed after the preliminary measurements and the system can be used by a real listener. A single loudspeaker was installed behind the active headrest system to act as the primary source and driven to produce either a sinusoidal sound or a stationary random sound.

For real-time tonal control, the optimal observation filters in the frequency domain were calculated from Eq. (4) with the pre-measured acoustic responses and the improved filtered-reference LMS algorithm suggested by [6] was applied for the integrated local active control. In addition, the performance for broadband control was estimated using offline simulations based on measured data using Eq. (15) and Eq. (17). The full set of transfer responses between the primary and secondary sources and the monitoring and physical error microphones was measured when the dummy head was located at 20 different positions on a 5 x 4 grid of points spaced 5 cm apart. Finally, a commercial head-tracking device, the Microsoft Kinect, was installed in front of the dummy head. The information from the Kinect was decoded in real time using a plug-in software implemented in MaxMSP and this

was passed to a dSPACE-based adaptive controller, which already had stored in it the various plant responses and pre-calculated observation filters for 20 head positions.

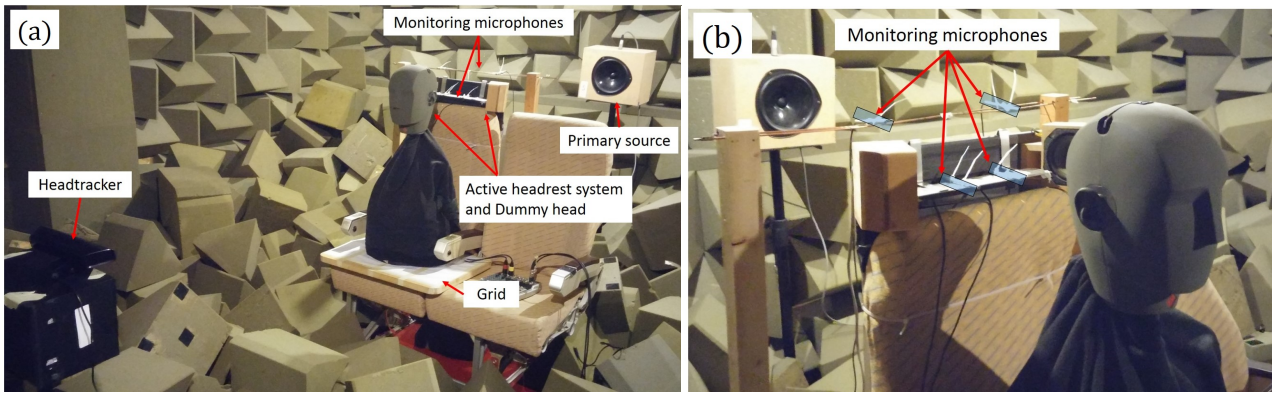

Figure 2: (a) The overall installation for both the nearfield estimation and the integrated active headrest system for controlling tonal disturbances in real-time and stationary random broadband disturbances in off-line (b) The positions of the 4 monitoring microphones

3.2 Real-time implementation for controlling tonal disturbances

When the regularization factor, β, in Eq. (4) was selected from the trade-off between the estimation accuracy and robustness to uncertainties as $\beta = 10^{-3}$, tonal disturbance signals at the error microphones of the dummy head at different frequencies were estimated from the monitoring microphone signals with the pre-calculated observation filter. The estimation error was defined as a normalised difference between acutal and estimated disturbance signals at the error microphones, as presented by [6]. Therefore, when the dummy head was located in the nominal position, the measured estimation errors in Table 1 show that tonal disturbance signals at the error microphones can be estimated with considerable accuracy. With this nearfield estimation accuracy, the achieved attenuation performance of the integrated active headrest system is also shown in Table 1. It is shown that attenuation performance of greater than 15 dB is achieved at different frequencies.

The effect of the head-tracking device on the integrated active control system was then investigated by moving the dummy head from the nominal position to different positions on the grid. When the dummy was moved 10 cm left, the time history of the signal measured at the right microphone in the dummy during control is shown in Fig. 3. It can be seen from Fig. 3 that when the active headrest system is implemented without the head tracker, the disturbance signal at 600 Hz is slightly reduced but the disturbance signal at 700 Hz is enhanced due to the significant difference between the virtual and actual error signals. However, when the head tracker is in operation, the attenuation performance is significantly improved at both frequencies.

Table 1: The real-time nearfield estimation error and attenuation performance of the integrated active headrest system when tonal disturbance signals at the error microphones of the dummy head in the nominal position are estimated by the 4 monitoring microphones around the headrest with the pre-calculated observation filter and are reduced by local active control in the anechoic chamber .

Frequencies	Real-time estimation error right / left ear, (dB)	Achieved attenuation performance right / left ear, (dB)
500 Hz	-19.3 / -15.1	-23.9 / -20.4
600 Hz	-21.1 / -17.1	-15.9 / -28.6
700 Hz	-17.0 / -16.0	-15.0 / -26.0

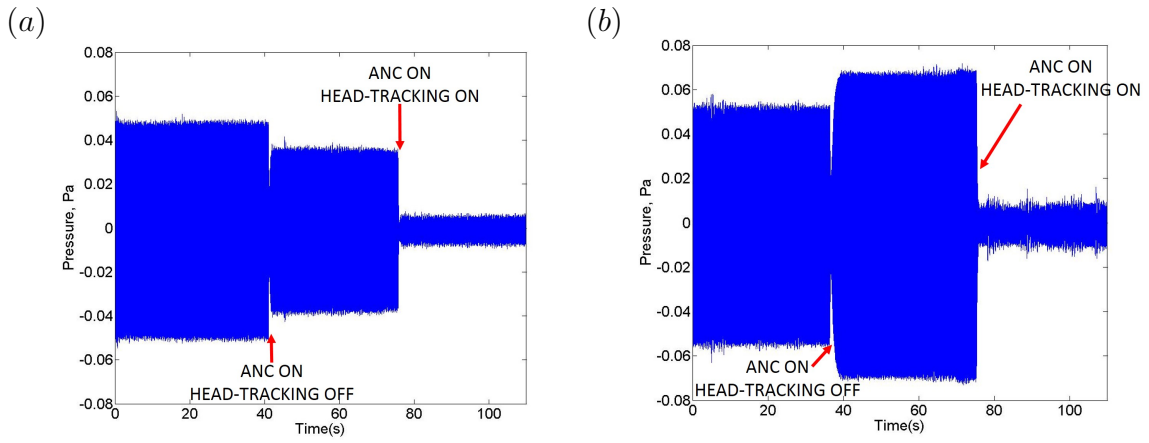

Figure 3: Measured signals at the right error microphone of the dummy head at a head position moved 10cm left from the nominal position when the integrated active headrest system with the remote microphone technique and the head tracker reduces the tonal disturbance signals from a single primary source in the anechoic chamber: (a) 600 Hz, (b) 700 Hz

3.3 Off-line predictions for the control of broadband random disturbances

When the primary source was driven to produce stationary random broadband sound, meausred signals from the monitoring and error microphones in Fig. 2 were used to investigate the attenuation performance of the active headrest system through off-line predictions. First of all, when the optimal observation filter with the causality constraint was obtained from Eq.(15), the impulse response of $\boldsymbol{O}_{12}$ among the FIR filters of $\boldsymbol{O}_{opt}$ is shown in Fig. 4 (a). When $\mathbf{O}_{12}$ of $\mathbf{O}_{opt}$ in Eq.(4) is transformed by inverse Fourier transform and compared with the impulse response of $\boldsymbol{O}_{12}$ of $\boldsymbol{O}_{opt}$ in Eq.(15), the impulse response of $\boldsymbol{O}_{12}$ is similar to the causal response of $\mathbf{O}_{12}$ but the noncausal response of $\mathbf{O}_{12}$ is excluded from the the impulse response of $\boldsymbol{O}_{12}$ due to the causality constraint. Fig. 4 (b) shows that the causally constrained filter can estimate stationary random disturbances at the error microphones with less than -10 dB estimation error except at around 250 Hz due to the corresponding anti-resonance.

The attenuation performance of the causally constrained controller is compared when the error signals are directly measured by the physical error microphones and are estimated by the causal observation filter. Although the attenuation performance with the remote microphone technique is generally lower than that of the physical error microphones, more than 10 dB is still achievable with the remote microphone technique. In this study, the causal nearfield estimation and active control achieve good performance because the primary source was behind the microphones and the noncausal response of the observation filter was thus relatively insignificant. However, if the primary source was located in front of the microphones, then the noncausal response would become more important and a modified remote microphone technique should be considered to overcome this problem.

4. Conclusions

The attenuation performance of an active headrest system integrated with the remote microphone technique and head-tracking has been investigated. The optimal observation filter and active controller have been initially derived in the frequency domain for controlling tonal disturbances. In addition, the optimal observation filter and active controller with a causality constraint have been formulated in the time domain for the sensing and control of broadband random disturbances. To improve the performance of these controllers, the head-tracking has also been suggested, when the position of a listener's head is changing. The nearfield estimation and noise reduction of the integrated system

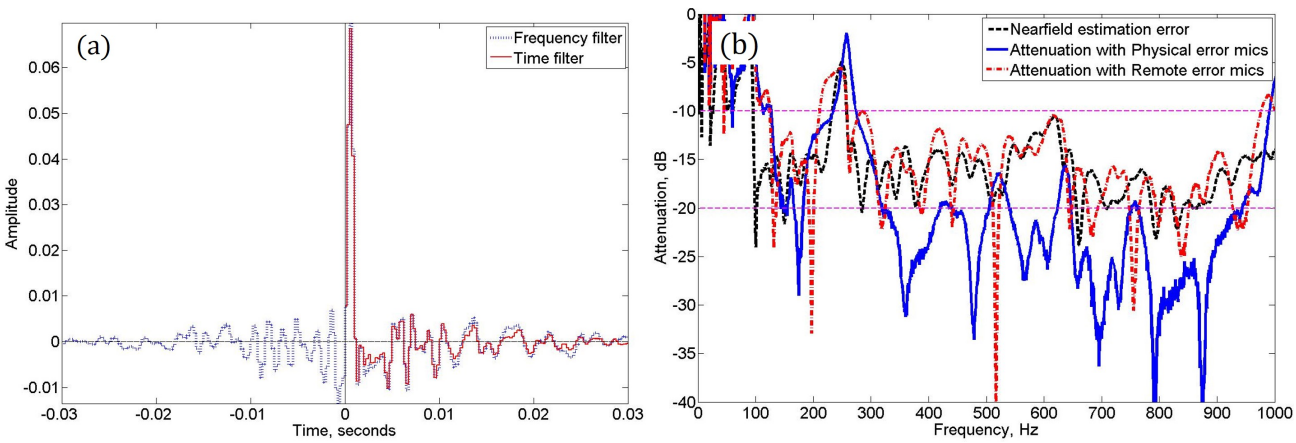

Figure 4: (a) Comparison of the impulse response of $\boldsymbol{O}_{12}$ among the FIR filters of the causal constrained $\boldsymbol{O}_{opt}$ with the inverse Fourier transformed $\mathbf{O}_{12}$ of $\mathbf{O}_{opt}$ without the causal constraint, (b) the nearfield estimation error(dash line) when a stationary random broadband sound is estimated by the monitoring microphones in Fig. 2 and the attenuation performance of the integrated active headrest system in Fig. 2 when the error signals are provided by either the physical error microphones (solid line) or the causal remote microphone technique(dash-dot line).

have been verified through real-time experiments for tonal control and off-line predictions for random broadband control. The real-time experimental results have demonstrated that disturbance signals at the error microphones were estimated by the monitoring microphones with less than -15 dB error and the adaptive active control achieved more than 15 dB attenuation. The application of a head-tracking device has improved the attenuation performance when the dummy head was moved to different positions from the nominal position. The results from the off-line predictions have shown that the causal filters for the nearfield estimation and active control achieve a reduction in the stationary random disturbances when noncausal responses are relatively insignificant.

Acknowledgement

This research is jointly funded by an EPSRC industrial CASE studentship and Jaguar Land Rover (JLR). The authors are especially thankful to Dr Delphine Nourzad of JLR for her support as an industrial supervisor.

REFERENCES

1. S. J. Elliott, *Signal Processing for Active Control*, (Academic Press, London) (2000).
2. M. Pawelczyk, "Adaptive noise control algorithms for active headrest system", Control Eng. Pract. **12**(9), 1101−1112 (2004).
3. A. Roure and A. Albarrazin, "The remote microphone technique for active noise control", in *Proceedings of INTER-NOISE and NOISE-CON Congress and Conference*, **1999**(5), 1233−1244 (1999).
4. S. J. Elliott and J. Cheer, "Modelling local active sound control with remote sensors in spatially random pressure fields", The Journal of the Acoustical Society of America **137**(4), 1936−1946 (2015).
5. D. Moreau, B. Cazzolato, A. Zander and C. Petersen, "A review of virtual sensing algorithms for active noise control", Algorithms **1**(2), 69−99 (2008).
6. W. Jung, S. J. Elliott and J. Cheer, "The effect of remote microphone technique and head-tracking on local active sound control", in *Proceedings of 23rd International Congress on Sound and Vibration*, July (2016).